RSC Advances

PAPER

View Article Online
View Journal | View Issue

Cite this: *RSC Adv.*, 2025, **15**, 30627

Design, synthesis, and *in silico* docking studies of novel cinnamaldehyde–chalcone derivatives with anti-cancer potential and *in vivo* acute oral toxicity profiling

A. Niranjana Kumar,[ag] G. Soumya,[b] V. Kanchana,[c] Kavita Singh,[d] Nidhi Maurya,[e] Sourabh Kumar,[d] Akanksha Singh,[e] J. Kotesh Kumar,[*a] K. V. N. S. Srinivas,[*a] Debabrata Chanda,[d] Suaib Luqman,[e] Sunil Misra,[c] Abha Meena[e] and B. Balakishan[f]

Cinnamaldehyde is a natural compound known for its antimicrobial and anticancer properties. Fourteen novel cinnamaldehyde–chalcone analogues (**5a–5n**) were synthesized and evaluated for anti-cancer, anti-bacterial, and anti-fungal activities. Among these, bromoethane chalcone **5n** exhibited significant cytotoxicity against DU145 (IC50: 8.719 ± 1.8 μM), SKBR-3 (IC50: 7.689 μM), and HEPG2 (IC50: 9.380 ± 1.6 μM) cell lines, surpassing other derivatives. Compounds para methyl benzyl chalcone **5j** and 2,3-dichloro benzyl chalcone **5b** also demonstrated notable activity against SKBR-3 (IC50 7.871 μM) and HEPG2 (IC50 9.190 μM) cell lines. Erythrocyte osmotic fragility (EOF) analysis showed higher erythrocyte fragility for **5n** (MEF_{50} = 0.457) and **5b** (MEF_{50} = 0.538), indicating membrane-disruptive potential compared to quercetin (MEF_{50} = 0.431). Studies on antimicrobial activity revealed that compounds **5a–5e** and **5n** demonstrated moderate effectiveness against *Staphylococcus aureus*, while compound **5l** showed activity against *Candida albicans* and *Candida tropicalis*. Docking studies revealed that compound **5n** binds to succinate dehydrogenase, a key enzyme in the TCA cycle, ETC, with greater affinity (−12.9 kcal mol^{-1}) than the standard inhibitor, malonate (−4.8 kcal mol^{-1}). Acute oral toxicity assessment of **5n** in Swiss albino mice demonstrated its safety at doses up to 1000 mg kg^{-1} body weight with no morbidity, mortality, or significant changes in haematological, biochemical, and pathological parameters. These findings highlight **5n**'s potential as a lead compound for further preclinical studies targeting cancer therapeutics.

Received 26th May 2025
Accepted 16th August 2025

DOI: 10.1039/d5ra03706a

rsc.li/rsc-advances

1. Introduction

Cinnamaldehyde 1 ((*E*)-3-phenylprop-2-enal) is a yellow oily liquid with a cinnamon odor and is derived from the inner bark of various trees from the genus *Cinnamomum*, which is made up of roughly 250 plant species.[1,2] The most common species are *C. cassia* (commonly referred to as Cassia) and *C. verum* (also called *C. zeylanicum*). These two species have different percentages of cinnamaldehyde, with up to 85.3% and 90.5% recorded, respectively. This aldehyde has been demonstrated to successfully suppress the development of an assortment of microorganisms such as bacteria, moulds, and yeasts. It has also been claimed to reduce toxin generation by microorganisms.[3,4] Cinnamaldehyde was accepted as Safe (GRAS) by the Flavour and Extract Manufacturer's Association (FEMA) and US-FDA and has been awarded a status set by the Council of Europe (*i.e.*, admissible use in food items).[5] On this premise, it may be seen as a safe food and flavour enhancer, with a pleasant taste and odour, and has found numerous commercial culinary applications.[6] Recently this molecule has been utilized as an agricultural fungicide.[7] It has also been used in edible antimicrobial films made from fruits and vegetables to kill foodborne germs by touch or vapours in closed containers.[8] This corresponds to an increasing interest in natural antimicrobials that not only inhibit the growth of foodborne pathogens and

[a]*Phytochemistry Division, CSIR-Central Institute of Medicinal and Aromatic Plants, Research Centre, Boduppal, Hyderabad-500092, India. E-mail: koteshkumarj@cimap.res.in; kvn.satyasrinivas@cimap.res.in; Fax: +91-40-27202602*

[b]*Centre for Pharmaceutical Sciences, JNTU College of Engineering Science and Technology, Jawaharlal Nehru Technological University, Hyderabad-500 085, India*

[c]*Department of Applied Biology, CSIR-Indian Institute of Chemical Technology, Hyderabad-500 007, India*

[d]*In-vivo Testing Facility, Bio-Prospection and Product Development, CSIR-Central Institute of Medicinal and Aromatic Plants, Lucknow-226 015, India*

[e]*Bio-Prospection and Product Development Division, CSIR-Central Institute of Medicinal and Aromatic Plants, Lucknow-226 015, India*

[f]*NMR Division, CSIR-Central Institute of Medicinal and Aromatic Plants, Lucknow-226 015, India*

[g]*Academy of Scientific and Innovative Research (AcSIR), Ghaziabad, Uttar Pradesh 201002, India*

spoiling bacteria but may also enhance the flavour and quality of foods.[9]

Extensive study has been conducted to investigate the vast variety of therapeutic potentials related with this compound and its natural and synthetic derivatives. Several outstanding studies have been reported about the pharmacological characteristics associated with the aldehyde itself,[2] as well as reviews on its derivatives and their related therapeutic benefits.[10] Cinnamaldehyde and its derivatives have been extensively studied for their possible anti-tumour and anti-cancer properties and has shown activity against a number of cancer cell lines, including A549, SK- OV -3, XF-498, HeLa, SK-MEL-2 and HCT-15 tumour cells.[11] A number of synthetic derivatives including 2-benzoyloxycinnamaldehyde, 4-hydroxycinnamaldehyde, 2-hydroxy-5-fluorocinnamaldehyde have demonstrated anti-cancer properties against leukemic, oral carcinoma, prostate and colon cancer cell lines.[12] Aside from its anti-tumour capabilities, these compounds have demonstrated other biological potentials like cardioprotective properties,[13] anti -inflammatory agents,[14] antifungal properties,[15] thermogenic effects,[16] antibacterial activity[17] *etc.* Recent structure–activity relationship studies on cinnamic acid derivatives bearing halogen substitutions and tertiary amine side chains have demonstrated enhanced acetylcholinesterase inhibition and improved selectivity over butyrylcholinesterase, suggesting the significance of strategic substitutions in modulating biological function and target selectivity.[18]

Chalcones are composed of two aryl moieties joined by an α, β-unsaturated carbonyl group.[19] These scaffolds, which are naturally present in fruits, spices, teas, and soy-based foods, have gained a lot of interest due to their fascinating and potentially beneficial qualities and present in natural products such as pheromones, plant allelochemicals, and insect hormones.[20,21] They undergo a variety of chemical processes and are used to produce heterocyclic compounds. Additionally these molecules serve as intermediary structures in biosynthetic pathways which generate flavonoids, isoflavonoids, and aurones.[22] A substantial part of medicinal chemistry research in the 21st century has been concentrated on both natural and synthetic chalcones because of their diverse pharmacological possibilities, such as anticancer,[23] antimalarial,[24] antidiabetic,[25] antiplatelet,[26] anti-inflammatory,[27] anticholinergic,[28] immunomodulatory,[29] analgesic,[30] antibacterial,[31] aldose reductase inhibition,[32] acetylcholinesterase inhibition,[33] antiviral,[34] non-purine xanthine oxidase inhibitors[35] *etc.* Additionally, hybrid chalcone frameworks bearing tertiary amine side chains have shown promising AChE/BChE inhibition profiles, reinforcing the pharmacological importance of substituent positioning and electronic effects structure–activity relationship investigation of coumarin–chalcone hybrids with diverse side-chains as acetylcholinesterase and butyrylcholinesterase inhibitors.[36]

Chalcones are highly attractive molecules because of their simple structure, ease of construction, and promising biological applications. Considering the significance of cinnamaldehyde derivatives and as part of our ongoing research work on synthesis of hybrid molecules[37–39] the aim of this study was to develop novel library of cinnamaldehyde–chalcone hybrids and evaluate their biological potential.

2. Results and discussion

2.1. Chemistry

The synthetic strategy followed for the synthesis of different cinnamaldehyde–chalcone analogues is outlined in Scheme 1. A series of compounds (**5a–n**) are synthesized in two steps. In the first step, cinnamaldehyde **1** was reacted with 2-hydroxyacetophenone 2 in the presence of sodium hydroxide as catalyst and ethanol as solvent yielded (2*E*, 4*E*)-1-(2-hydroxyphenyl)-5-phenylpenta-2,4-dien-1-one **3** by aldol condensation. In the second step **3** was reacted with different substituted benzyl/alkyl bromides/chlorides (**4a–n**) in the presence of dimethyl formamide (DMF) as solvent and potassium carbonate (K_2CO_3) at room temperature for 5 h to give brominated/alkylated derivatives **5a–n** in pure form. In the case of compound **5n**, the monomeric form was obtained predominantly, with only trace amounts of the corresponding dimer. This is attributed to the mild basic conditions employed in the Claisen–Schmidt condensation, which favour monomer formation. All the synthesized compounds were characterized by spectroscopy such as IR, ^{1}H, and ^{13}C NMR and mass. In the ^{1}H NMR of compound **3**, the aldehyde peak was absent at δ 9.77 ppm and hydroxyl proton was appeared at δ 12.88 ppm indicates that aldehyde group was condensate with acetophenone group of compound **2**. Similarly, in ^{13}C NMR presence of peak resonances at δ 193.71 ppm indicate that chalcone ketone group was present in the molecule and all aromatic carbons was appeared between δ 118–163 ppm.

The DEPT-135 NMR spectrum confirmed the presence of four quaternary carbon atoms in the synthesized molecules. This was further supported by the mass spectrum, where the molecular ion peak (M + 1) was observed at *m*/*z* 251, corresponding to the molecular formula $C_{17}H_{14}O_2$. In the ^{1}H NMR spectrum of compound **5d**, a triplet resonance at δ 5.24 ppm indicated coupling between the 2-chlorobenzyl group and the OH proton of intermediate compound **3**. This was further validated by the ^{13}C NMR spectrum, which showed the –CH_2- carbon signal at δ 69.45 ppm. The carbonyl group of the

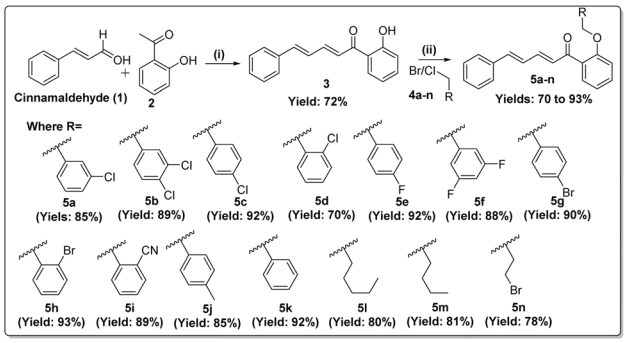

Scheme 1 General scheme for synthesis of cinnmaldehyde–cahlcone analogues (**5a–5n**). [Reaction Conditions: (i)- NaOH, ethanol, RT, 4 h; (ii)- DMF, K_2CO_3, RT, 4 h].

chalcone moiety resonated at δ 192.72 ppm. All other proton and carbon signals appeared in their expected chemical shift regions. The LC-MS spectrum of the final compound **5d** displayed a molecular ion peak $[M + H]^+$ at m/z 375.1151, consistent with the molecular formula $C_{24}H_{19}ClO_2$.

2.2. Anti-cancer activity

2.2.1. Effect of cinnmaldehyde–cahlcone conjugates on cell viability – MTT assay. Anticancer activity of the synthesized cinnmaldehyde–cahlcone analogues (**5a–5n**) was evaluated *in vitro* mode using 3-(4,5-dimethylthiazol-2-yl)-2,5-diphenyltetrazolium bromide (MTT) assay on the HEK-293 (human embryonic kidney cell line), DU145 (human prostate cell line), SKBR-3 (human breast cancer cell line) and HepG2 (Human hematoma cell line). The assay was based on the reduction of MMT by the mitochondrial dehydrogenase of viable cells into purple formazan crystals which get dissolved in DMSO and measured at 570 nm. The results of cytotoxic activity *in vitro* were expressed as the IC_{50} (μM) and doxorubicin was used as positive control (Table 1). The structural diversity in all the derivatives was introduced by varying substitution at chalcone 'O' position of the chalcone moiety intact.

As shown in Table 1, most of the tested compounds exhibited moderate cytotoxic activity. However, bromoethyl chalcone **5n** demonstrated the highest toxicity, particularly against DU145 (IC_{50}: 8.719 ± 1.8 μM), SKBR-3 (IC_{50}: 7.689 ± 2.8 μM), and HEPG2 (IC_{50}: 9.380 ± 1.6 μM), though it remained less potent than the standard doxorubicin (IC_{50}: 0.45 ± 0.52, 0.7 ± 0.56, and 2.5 ± 1.42 μM, respectively). Similarly, para-methyl benzyl chalcone **5j** showed notable cytotoxicity against SKBR-3 (IC_{50}: 7.871 ± 2.1 μM), and 2,3-dichloro benzyl chalcone **5b** was highly toxic to HEPG2 (IC_{50}: 9.190 ± 0.6 μM), though both remained less effective than doxorubicin (IC_{50}: 0.7 ± 0.56 and 2.5 ± 1.42 μM, respectively). Additionally, 4-bromo benzyl chalcone **5g** exhibited moderate toxicity toward DU145 (IC_{50}: 16.914 ± 2.3 μM) and SKBR-3 (IC_{50}: 15.711 ± 2.8 μM) compared to doxorubicin (IC_{50}: 0.45 ± 0.52 and 0.7 ± 0.56 μM, respectively). The starting compound, cinnamaldehyde **1**, displayed moderate cytotoxicity across all four cell lines, with IC_{50} values of 20.572 ± 1.0 μM (HEK-293), 22.354 ± 1.6 μM (DU145), 13.901 ± 1.6 μM (SKBR-3), and 21.840 ± 1.0 μM (HEPG2), but was still less potent than doxorubicin (IC_{50}: 6.12 ± 0.5, 0.45 ± 0.52, 0.7 ± 0.56, and 2.5 ± 1.42 μM, respectively). The observed activity for select compounds can be rationalized based on the structure–activity relationship. Only compounds with specific substitutions, such as electron-withdrawing groups (*e.g.*, halogens) or lipophilic chains at the benzyl position—like in **5n**, **5j**, and **5b**—demonstrated enhanced cytotoxicity. These structural features likely improve membrane permeability and target affinity. In contrast, compounds lacking such moieties may suffer from poor cellular uptake, steric hindrance, or suboptimal interaction with the biological target, leading to their diminished activity.

2.2. *In vivo* acute oral toxicity of compound 5n

Further studied the Acute Oral Toxicity Assessment of **5n** in Swiss Albino Mice (Observational, haematological, biochemical and gross pathological study). Table 2 and Fig. 1 present the acute oral toxicity assessment of compound **5n** in Swiss albino mice, evaluating its impact on body weight, hematological, biochemical, and organ parameters at doses of 5, 50, 300, and 1000 mg kg^{-1}.[40] Throughout the study, no morbidity, mortality, or abnormal clinical signs were observed, indicating a high tolerance to the compound. Body weight changes across different dose groups remained within a normal range, with no statistically significant alterations compared to the control. Hematological parameters, including hemoglobin, RBC, and WBC counts, showed no significant deviations, although a slight increase in WBC count was noted at the highest dose (1000 mg kg^{-1}), suggesting a mild physiological response.

Table 1 Anti-cancer activity of compounds **5a–5n**

	Cell lines (IC_{50} μM)			
Compound	HEK-293	DU145	SKBR-3	HEPG2
1	20.572 ± 1.0	22.354 ± 1.6	13.901 ± 1.6	21.840 ± 1.0
3	67.392 ± 9.1	83.457 ± 7.3	20.834 ± 4.1	40.094 ± 2.0
5a	30.092 ± 8.3	45.217 ± 2.1	20.839 ± 1.7	40.322 ± 2.9
5b	20.391 ± 1.6	17.861 ± 3.4	22.421 ± 2.4	9.190 ± 0.6
5c	22.321 ± 1.2	47.064 ± 4.5	30.745 ± 2.0	40.170 ± 0.2
5d	202.78 ± 5.3	46.055 ± 1.1	75.883 ± 4.8	41.449 ± 3.9
5e	49.837 ± 2.8	278.60 ± 1.7	56.126 ± 1.8	282.42 ± 5.7
5f	36.978 ± 0.9	47.073 ± 0.5	16.898 ± 2.3	30.825 ± 2.5
5g	27.588 ± 4.2	16.914 ± 2.3	15.711 ± 2.8	25.825 ± 1.6
5h	23.387 ± 4.7	28.630 ± 2.2	243.79 ± 4.7	44.965 ± 3.3
5i	48.182 ± 5.0	68.374 ± 2.8	75.293 ± 2.1	42.012 ± 2.1
5j	23.570 ± 1.4	21.260 ± 5.6	7.871 ± 2.1	25.678 ± 1.5
5k	109.383 ± 0.7	55.586 ± 3.7	80.336 ± 8.7	46.573 ± 1.4
5l	97.976 ± 10.1	29.036 ± 2.1	23.466 ± 4.1	46.681 ± 2.2
5m	104.184 ± 7.3	126.83 ± 0.2	125.34 ± 6.0	33.159 ± 0.7
5n	18.461 ± 1.1	8.719 ± 1.8	7.689 ± 2.8	9.380 ± 1.6
Doxorubicin	6.12 ± 0.5	0.45 ± 0.52	0.7 ± 0.56	2.5 ± 1.42

Table 2 Effect of **5n** as a single acute oral dose at 5, 50, 300, and 1000 mg kg^{-1} on body weight, haematology and serum biochemical parameters in Swiss albino mice (mean ± SE; $n = 6$)

	Dose of **5n** at mg per kg body weight as a single oral dose				
Parameters	Control	5 mg kg^{-1}	50 mg kg^{-1}	300 mg kg^{-1}	1000 mg kg^{-1}
Body weight (g)	32.47 ± 0.61	31.33 ± 1.54	28.33 ± 0.72	31.82 ± 0.96	27.92 ± 1.30
Haemoglobin (g dL^{-1})	12.60 ± 0.93	12.74 ± 0.51	12.68 ± 0.67	12.68 ± 0.71	12.42 ± 0.55
RBC (million per mm^3)	8.06 ± 0.65	8.20 ± 0.60	7.77 ± 0.66	7.34 ± 0.38	7.54 ± 0.62
WBC (1000*/mm^3)	9.34 ± 1.12	9.48 ± 0.68	9.54 ± 0.79	10.13 ± 0.50	12.17 ± 0.95
ALKP (U L^{-1})	175.91 ± 11.21	170.67 ± 13.43	164.25 ± 13.54	173.23 ± 14.47	170.75 ± 6.26
SGOT (U L^{-1})	22.97 ± 1.37	20.84 ± 0.88	20.60 ± 1.71	19.39 ± 1.51	19.73 ± 1.43
SGPT (U L^{-1})	19.77 ± 1.48	16.76 ± 0.67	18.63 ± 0.59	18.03 ± 0.64	17.55 ± 1.23
Albumin (g dL^{-1})	2.72 ± 0.06	2.55 ± 0.19	2.58 ± 0.07	2.55 ± 0.19	2.70 ± 0.09
Creatinine (mg dL^{-1})	0.95 ± 0.12	0.92 ± 0.08	0.86 ± 0.06	0.90 ± 0.13	0.97 ± 0.09
Triglycerides (mg dL^{-1})	109.44 ± 3.01	111.43 ± 4.39	111.02 ± 5.61	110.41 ± 3.90	108.74 ± 2.77
Serum protein (mg mL^{-1})	5.47 ± 0.18	5.85 ± 0.13	5.76 ± 0.16	5.86 ± 0.18	5.93 ± 0.13
Cholesterol (mg dL^{-1})	111.87 ± 5.03	113.94 ± 4.49	110.16 ± 3.57	111.51 ± 3.48	107.82 ± 3.48
Bilirubin (mg dL^{-1})	0.52 ± 0.00	0.50 ± 0.00	0.51 ± 0.00	0.49 ± 0.02	0.47 ± 0.04

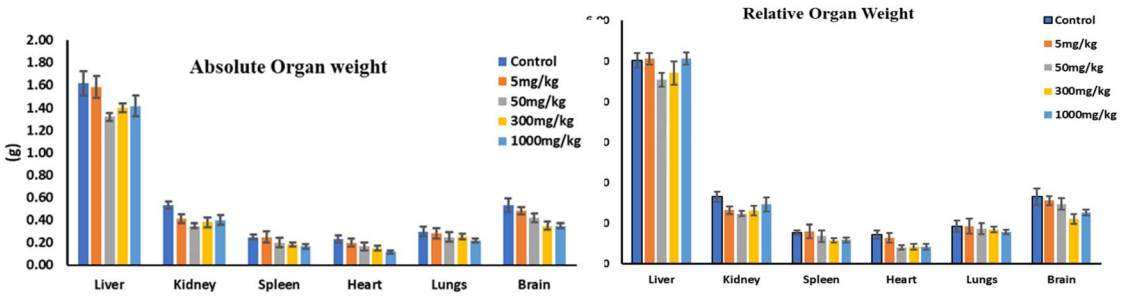

Fig. 1 Effect of **5n** as a single acute oral dose at 5, 50, 300, and 1000 mg kg^{-1} on absolute and relative organ weight in Swiss albino mice (mean ± SE; $n = 6$; *, $P < 0.001$ compared to control).

Biochemical markers such as ALKP, SGOT, SGPT, albumin, creatinine, triglycerides, serum protein, cholesterol, and bilirubin exhibited no significant changes, further supporting the compound's safety profile. Gross pathological examination and organ weight analysis (Fig. 1) revealed no significant abnormalities in absolute or relative organ weights, reinforcing the absence of toxicity-related organ damage. The overall findings suggest that compound **5n** is well tolerated up to 1000 mg kg^{-1} as a single acute oral dose, with no adverse effects on physiological, hematological, or biochemical parameters, making it a promising candidate for further preclinical evaluation.

2.3. Erythrocyte osmotic fragility (EOF)

The erythrocyte osmotic fragility (EOF) of **5b** and **5n** derivatives was evaluated. The EOF curve illustrates the percentage of hemolysis at varying Phosphate-Buffered Saline (PBS) concentrations. The control group (black) exhibits the least fragility, while compound **5n** (red) shows the utmost hemolysis, indicating increased erythrocyte fragility and potential membrane-disrupting effects. Compound **5b** (blue) follows a similar trend but with slightly lower hemolysis. quercetin (green) and DMSO (purple) provide moderate protection (Fig. 2). The Mean Erythrocyte Fragility at 50% hemolysis (MEF_{50}) values are presented in Table 3. Compound **5b** exhibited the highest MEF_{50} = 0.538, followed by **5n** (0.457). Quercetin-treated cells (used as a positive control) had an MEF_{50} of 0.431, closer to compound **5b**. Recent evidence suggests that targeting post-translational regulators like palmitoyl-protein thioesterase 1 (PPT1), which modulates protein palmitoylation and MAPK signaling, may overcome chemoresistance in osteosarcoma, and the apoptotic and membrane-disruptive effects of compound **5n** may align with such mechanisms, warranting further mechanistic investigation.[41]

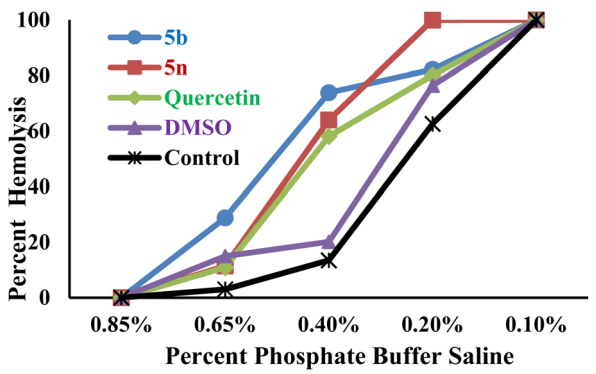

Fig. 2 Erythrocyte osmotic fragility curve of cinnamaldehyde–chalcone derivatives, dimethyl sulphoxide (DMSO).

Table 3 Mean Erythrocyte Fragility (MEF_{50}) of active derivatives of cinnamaldehyde[a]

Sample	MEF_{50}
5b	0.538
5n	0.457
Quercetin	0.431
DMSO	0.266
Control	0.236

[a] MEF_{50} concentration of PBS at which 50% of erythrocytes undergo hemolysis.

2.4. Molecular docking studies

Molecular docking is a vital computational tool in drug development, used to assess the therapeutic potential of compounds by predicting their binding affinity, interactions, and stability with target proteins. Key non-covalent interactions ionic, hydrogen bonding, van der Waals forces, and hydrophobic effects, govern molecular interactions.[42] In this study, synthesized compounds were docked with succinate dehydrogenase (SDH), a crucial enzyme in the TCA cycle and electron transport chain. Beyond its role in energy metabolism, SDH has gained attention for its involvement in cancer cell survival, particularly in relation to hereditary cancer-linked mutations.[43] To further explore these interactions, molecular docking of the most active compound, **5n**, was carried out using SDH (PDB ID: 6VAX) as the receptor.[39] The docking results were compared with malonate, a known SDH ligand, to assess the binding site overlap and relative affinity.[44] As shown in Table 4, compound **5n** exhibited a remarkably high binding affinity with a docking energy of −12.9 kcal mol^{-1} and a calculated inhibition constant (K_i) of 3.44×10^{-10} μM, indicating strong and potentially irreversible binding to the SDH active site. In comparison, malonate showed a significantly lower binding energy of −4.8 kcal mol^{-1} and a K_i of 3.01×10^{-4} μM. The interaction mapping of **5n** within the SDH binding pocket revealed multiple hydrophobic and polar contacts. Key residues involved include ASP561, THR560, ARG67, GLU64, LEU94, ALA68, LEU71, LEU161, LEU158, PHE162, and ASP553. Notably, LEU158 and ASP561 were also found in the binding site of the reference ligand malonate, indicating a partial overlap in binding pockets and potential competitive inhibition. Interestingly, unlike malonate, which formed hydrogen bonds with residues such as SER509, THR508, LEU158, and ARG512, compound **5n** did not show classical hydrogen bonding interactions but instead exhibited strong van der Waals and hydrophobic interactions, particularly with multiple leucine residues (LEU94, LEU158, LEU161, LEU71), and π–π stacking with PHE162. These interactions are visualized in Fig. 3C and D, which illustrate the 3D and 2D docking poses of **5n**-SDH, respectively. The robust binding affinity of **5n** is likely driven by its extended aromatic system and lipophilic side chains, which allow deeper insertion into the hydrophobic core of the SDH binding cavity. The absence of H-bonding is compensated by strong hydrophobic contacts and electrostatic interactions, particularly with charged residues like ARG67 and ASP553. These findings underscore the potential of **5n** as a potent SDH inhibitor.

2.5. Anti-microbial activity

The Anti-bacterial and anti-fungal Activities were also studied for the synthesized analogues. Table S1 and Fig. S1 & S2 present the antibacterial and antifungal activity of synthesized analogues at 18 hours, measured as the zone of inhibition (mm) at 1 mg mL^{-1}. **1** exhibited the broadest activity, inhibiting all tested bacteria (*Escherichia coli*, *Klebsiella pneumoniae*, *Staphylococcus aureus*, *Bacillus subtilis*) with zones of 7–8 mm, and both fungi (*Candida albicans* and *Candida tropicalis*) with 11 mm inhibition. Several compounds (**3**, **5a–5e**, and **5n**) selectively inhibited *Staphylococcus aureus* (7 mm), while **5m** was active only against *Klebsiella pneumoniae* (8 mm). Sample **5l** showed antifungal activity (8 mm for *Candida albicans*, 7 mm for *Candida tropicalis*) (Fig. S2), but most analogues (**5f–5k**) exhibited no activity. Compared to standard antibiotics (streptomycin 24 mm for bacteria, ketoconazole 24 mm for fungi), the synthesized compounds showed moderate to weak potency, with **1** demonstrating the most promising broad-spectrum activity.

3. Experimental

3.1. Chemistry

All other chemicals and reagents purchased from Aldrich (India), AVRA Chemicals Pvt. Ltd. (India) and were used without further purification. TLC Silica gel 60 F_{254} (Merck, Germany) was used for TLC. Visualization of the developed TLC was

Table 4 Represents the binding energy, inhibition constant, and binding site of ligand **5n** and malonate with SDH receptor protein (highlighted residue showing the similar binding residue with the standard ligand (malonate))

Receptor (PDB ID)	Ligand	Binding energy (kcal mol^{-1})	K_i (μM)	Binding pockets	H-bond (Å)
SDH (6VAX)	**5n**	−12.9	3.44281×10^{-10}	**ASP561**, THR560, ARG67, GLU64, LEU94, ALA68, LEU71, LEU161, **LEU158**, PHE162, ASP553	—
	Malonate	−4.8	3.01198×10^{-4}	GLU564, ARG507, ARG512, LEU158, LYS550,GLU159, THR508, ASP561, SER509	SER509 (3.4), THR508 (3.4), LEU158 (3.6), ARG512 (4.8)

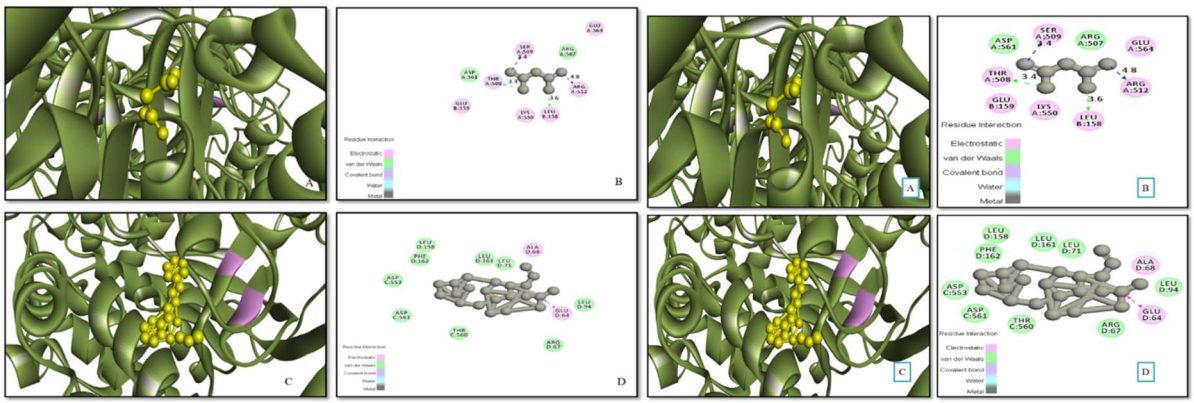

Fig. 3 (A) Represents the 3D interaction of docked complex of Malonate-SDH (B) 2D representation of the binding pockets of Malonate. (C) Represents the 3D interaction of docked complex of **5n**-SDH (D) 2D representation of the binding pockets of **5n**.

performed by UV light or 5% H_2SO_4 in MeOH stain. Melting points were measured using A. KRUSS OPTRONIC (Germany) melting point apparatus and are uncorrected. IR spectra were recorded on a Bruker Optics (Tensor 27 model, Germany) FT-IR spectrophotometer (using KBr pellets) and reported in wave number (cm^{-1}). ^1H NMR (400/500 MHz) and ^{13}C NMR (75/100 MHz) spectra were measured in $CDCl_3$ and DMSO-d_6 at room temperature on a Bruker Avance-III 400/500 MHz (Switzerland) instruments. The Chemical shifts are reported as δ parts per million (ppm) in $CDCl_3$ (δ_H = 7.26; δ_C = 77.0) using tetramethylsilane as an internal standard. Data are reported as follows: chemical shift, multiplicity (s: singlet, d: doublet, t: triplet, dd: doublet of doublet, q: quartet, br: broad, m: multiplet), coupling constants (J in Hz) and integration.

3.2 General procedure for synthesis of cinnamaldehyde–chalcone-analogues

3.2.1 Synthesis of (2*E*,4*E*)-1-(2-hydroxyphenyl)-5-phenylpenta-2,4-dien-1-one (3). Cinnamldehyde **1** (1.0 g, 7.575 m moles) and 2-hydroxyacetophenone (**2**, 0.925 g, 1.0 eq.) are dissolved in 20 mL of ethanol. To this reaction mixture added NaOH (1.5 eq.) and the reaction was carried out at 35–40 °C for 4 h. Then reaction mixture was diluted with ice cold distilled water (500 mL) and stirred for 15 min, resulted solid filtered off, washed with water then with methanol, and recrystallized form petroleum ether to get yellow needles of (2*E*,4*E*)-1-(2-hydroxyphenyl)-5-phenylpenta-2,4-dien-1-one (**3**) in pure from.

3.3 *O*-Alkylation/benzylation of compound 3

Compound **3** (0.3 g, 1.2 m moles) along with 0.246 g (1.5 equiv.) of anhydrous potassium carbonate was taken in 20 mL of dimethyl formamide (DMF) in clean RB flask and added slowly alkyl bromides or chlorides/benzyl bromides or chlorides (**4a–n**, 1.5 equiv.) to this solution. Reaction mixture was stirred at RT for 4 h to afford crude *O*-alkylated/benzylated derivatives. This crude compound was poured in to distilled water (500 mL), filtered then washed with water and dried to yield pure alkylated/benzylated derivatives (**5a–n**) of 2-(2*E*, 4*E*)-1-(2-hydroxyphenyl)-5-phenylpenta-2,4-dien-1-one (**3**) in quantitative yields.

3.3.1 Spectral data of synthesized compounds compound 3 [(2*E*,4*E*)-1-(2-hydroxyphenyl)-5-phenylpenta-2,4-dien-1-one]. Yield: 800 mg (72%), yellow solid, IR. (KBr): 3957, 3857, 3855,3257, 2401, 2010, 825 cm^{-1}; ^1H NMR (400 MHz, $CDCl_3$): δ_H (ppm) 12.88 (s, 1H), 7.84 (dd, J = 8.1, 1.6 Hz, 1H), 7.71 (ddd, J = 14.7, 7.4, 2.9 Hz, 1H), 7.53 (m, 3H), 7.41 (m, 3H), 7.26 (m, 1H), 7.08 (m, 3H), 6.92 (ddd, J = 8.2, 7.3, 1.1 Hz, 1H) (Fig. S3); ^{13}C NMR (100 MHz, $CDCl_3$): δ_c (ppm) 193.71, 163.60, 145.52, 142.93, 136.25, 135.97, 129.52, 129.51, 128.93, 127.46, 126.70, 123.48, 120.04, 118.80, 118.60 (Fig. S4); ESI-MS: positive ion mode: m/z = 251 $[M + H]^+$ calculated mass (M) for $C_{17}H_{14}O_2$ is 250.30. (Fig. S5)

3.3.2 (2*E*,4*E*)-1-(2-((3-Chlorobenzyl)oxy)phenyl)-5-phenylpenta-2,4-dien-1-one (5a). Yield: 250 mg (85%), yellow solid, m.p. 144–146 °C; IR (KBr): 3092, 3019, 2940, 2338, 1951, 1886, 1794, 1641, 1591, 1567, 1437, 1344, 1283, 1230, 1154, 1098, 991, 875, 753, 681 cm^{-1}; ^1H NMR (500 MHz, $CDCl_3$) δ 7.63 (dd, J = 7.6, 1.7 Hz, 1H), 7.46 (m, 5H), 7.36 (m, 3H), 7.31 (m, 3H), 7.27 (m, 2H), 7.07 (td, J = 7.5, 0.7 Hz, 1H), 7.01 (m, 1H), 6.93 (m, 2H), 5.14 (s, 2H) (Fig. S6). ^{13}C NMR (100 MHz, $CDCl_3$): δ_c (ppm): 192.80, 156.78, 143.61, 141.39, 138.54, 132.73, 130.67, 130.55, 129.89, 129.87, 129.06, 128.79, 128.12, 127.27, 127.16, 127.06, 125.12, 121.06, 113.04, 69.86 (Fig. S7).; LC-MS: positive ion mode: m/z = 375.1153 $[M + H]^+$ calculated mass (M) for $C_{24}H_{19}ClO_2$ is 374.8640 (Fig. S8).

3.3.3 (2*E*,4*E*)-1-(2-((3,4-dichlorobenzyl)oxy)phenyl)-5-phenylpenta-2,4-dien-1-one (5b). Yield: 291 mg (89%), yellow solid, m.p. 239–241 °C; IR (KBr): 3107, 3044, 2964, 1909, 1664, 1619, 1577, 1500, 1410, 1362, 1305, 1257, 1185, 1129, 1041, 884, 812, 719, 642 cm^{-1}; ^1H NMR (500 MHz, $CDCl_3$) δ 7.58 (s, 2H), 7.49 (m, 5H), 7.38 (m, 4H), 7.08 (dd, J = 16.8, 10.3 Hz, 2H), 7.02 (m, 3H), 5.14 (d, J = 1.3 Hz, 2H) (Fig. S9). ^{13}C NMR (100 MHz, $CDCl_3$): δ_c (ppm): 192.65, 156.34, 143.64, 141.41, 136.73, 135.91, 132.67, 130.43, 130.14, 129.63, 129.06, 128.92, 128.72, 127.13, 126.77, 126.33, 112.99, 69.02 (Fig. S10). LC-MS: positive ion mode: m/z = 409.0763 $[M]^+$ calculated mass (M) for $C_{24}H_{18}Cl_2O_2$ is 409.3060 (Fig. S11).

3.3.4 (2*E*,4*E*)-1-(2-((4-Chlorobenzyl)oxy)phenyl)-5-phenylpenta-2,4-dien-1-one (5c). Yield: 320 mg (92%), yellow solid, m.p. 204–206 °C; IR (KBr): 3018, 2955, 2917, 2869, 1733, 1659, 1611, 1494, 1458, 1370, 1301, 1253, 1214, 1086, 1038, 922, 853, 753, 667 cm^{-1}; ^1H NMR (500 MHz, $CDCl_3$) δ (ppm): 7.65 (dd, J = 7.6, 1.8 Hz, 1H), 7.49 (m, 3H), 7.40 (m, 8H), 7.09 (td, J = 7.5, 0.8 Hz, 2H), 7.03 (d, J = 8.3 Hz, 1H), 6.95 (dd, J = 15.4, 7.6 Hz, 1H), 6.87 (dd, J = 15.5, 10.8 Hz, 1H), 5.16 (s, 2H) (Fig. S12). ^{13}C NMR (100 MHz, $CDCl_3$): δ_c (ppm): 192.81, 156.88, 143.51, 141.25, 136.16, 134.98, 133.84, 132.69, 130.80, 130.48, 129.78, 129.11, 128.87, 128.78, 128.58, 127.21, 127.03, 121.36, 113.15, 69.96 (Fig. S13). LC-MS: positive ion mode: m/z = 375.1150 $[M + H]^+$ calculated mass (M) for $C_{24}H_{19}ClO_2$ is 374.8640 (Fig. S14).

3.3.5 (2*E*,4*E*)-1-(2-((2-Chlorobenzyl)oxy)phenyl)-5-phenylpenta-2,4-dien-1-one (5d). Yield: 315 mg (70%), yellow solid, m.p. 247–249 °C; IR (KBr): 2941, 2857, 2810, 1793, 1642, 1600, 1402, 1237, 1082, 999, 871, 711, 657 cm^{-1}; ^1H NMR (400 MHz, $CDCl_3$): δ_H (ppm) 8.31 (s, 1H), 7.57 (dd, J = 7.0, 1.5 Hz, 1H), 7.55 (m, 1H), 7.52 (d, J = 1.8 Hz, 2H), 7.48 (dd, J = 7.6, 1.7 Hz, 1H), 7.44 (m, 2H), 7.38 (d, J = 2.4 Hz, 1H), 7.37 (m, 1H), 7.28 (m, 1H), 7.26 (m, 1H), 7.13 (s, 1H), 7.12 (m, 1H), 7.09 (d, J = 0.8 Hz, 1H), 6.98 (s, 1H), 6.94 (s, 1H), 5.24 (s, 2H) (Fig. S15).; ^{13}C NMR (100 MHz, $CDCl_3$): δ_c (ppm) 192.72, 156.46, 143.88, 141.89, 139.69, 136.50, 133.63, 133.28, 131.03, 130.72, 130.02, 129.62, 129.33, 128.22, 127.72, 127.54, 126.52, 121.53, 113.95, 69.45 (Fig. S16).; LC-MS: positive ion mode: m/z = 375.1151 $[M + H]^+$ calculated mass (M) for $C_{24}H_{19}ClO_2$ is 374.8640 (Fig. S17).

3.3.6 (2*E*,4*E*)-1-(2-((4-Fluorobenzyl)oxy)phenyl)-5-phenylpenta-2,4-dien-1-one (5e). Yield: 330 mg (92%), yellow solid, m.p. 219–221 °C; IR (KBr): 3011, 2938, 2884, 2852, 2785, 2345, 2312, 1512, 1401, 1356, 1131, 997, 873, 713 cm^{-1}; ^1H NMR (400 MHz, $CDCl_3$): δ_H (ppm): 7.99 (dd, J = 8.2, 1.6 Hz, 1H), 7.63 (dd, J = 8.1, 6.6 Hz, 3H), 7.58 (m, 4H), 7.43 (m, 3H), 7.29 (m, 2H), 7.20 (m, 1H), 7.10 (m, 1H), 7.00 (ddd, J = 7.1, 5.7, 4.5 Hz, 1H), 6.91 (dd, J = 15.1, 8.9 Hz, 1H), 5.21 (s, 2H) (Fig. S18); LC-MS: positive ion mode: m/z = 359.1440 $[M + H]^+$ calculated mass (M) for $C_{24}H_{19}FO_2$ is 358.4124 (Fig. S19).

3.3.7 2*E*,4*E*)-1-(2-((3,5-Difluorobenzyl)oxy)phenyl)-5-phenylpenta-2,4-dien-1-one (5f). Yield: 298 mg (88%), yellow solid, m.p. 189–191 °C; IR (KBr): 3059, 2938, 2884, 2789, 2317, 1796, 1637, 1595, 1441, 1349, 1317, 1232, 1111, 998, 961, 866, 737, 676 cm^{-1}; ^1H NMR (400 MHz, $CDCl_3$): δ_H (ppm): 7.64 (dd, J = 7.6, 1.8 Hz, 1H), 7.50 (m, 7H), 7.11 (td, J = 7.5, 0.8 Hz, 1H), 7.00 (m, 6H), 6.75 (ddd, J = 8.9, 5.6, 2.3 Hz, 1H), 5.16 (s, 2H) (Fig. S20); ^{13}C NMR (100 MHz, $CDCl_3$): δ_c (ppm): 192.89, 164.11, 1162.23, 156.38, 143.98, 141.67, 140.55, 136.17, 132.62, 130.53, 130.43, 129.94, 129.13, 128.80, 127.27, 126.83, 121.63, 112.98, 109.73, 109.53, 103.49, 103.29, 69.36 (Fig. S21); LC-MS: positive ion mode: m/z = 377.1363 $[M + H]^+$ calculated mass (M) for $C_{24}H_{18}F_2O_2$ is 376.4028 (Fig. S22).

3.3.8 (2*E*,4*E*)-1-(2-((4-Bromobenzyl)oxy)phenyl)-5-phenylpenta-2,4-dien-1-one (5g). Yield: 305 mg (90%), yellow solid, m.p. 194–196 °C; IR (KBr): 3050, 2875, 2305, 1932, 1793, 1640, 1591, 1475, 1343, 1287, 1235, 1152, 1104, 1066, 992, 871, 804, 737, 681 cm^{-1}; ^1H NMR (400 MHz, $CDCl_3$): δ_H (ppm): 7.85 (d, J = 2.8 Hz, 1H), 7.58 (m, 4H), 7.50 (m, 2H), 7.45 (m, 5H), 7.38 (m, 1H), 7.26 (dt, J = 15.2, 6.5 Hz, 2H), 7.11 (m, 2H), 6.93 (d, J = 15.1 Hz, 1H), 5.21 (s, 2H) (Fig. S23); ^{13}C NMR (100 MHz, $CDCl_3$): δ_c (ppm): 192.83, 163.09, 156.64, 143.30, 141.10, 131.48, 130.62, 128.95, 128.73, 127.04, 126.80, 121.59, 121.14, 112.97, 112.30, 69.69 (Fig. S24).; LC-MS: positive ion mode: m/z = 419.0641 $[M]^+$ calculated mass (M) for $C_{24}H_{19}BrO_2$ is 419.3180 (Fig. S25).

3.3.9 (2*E*,4*E*)-1-(2-((2-Bromobenzyl)oxy)phenyl)-5-phenylpenta-2,4-dien-1-one (5h). Yield: 322 mg (93%), yellow solid, m.p. 230–232 °C; IR (KBr): 3779, 3367, 3244, 2623, 2495, 2379, 1762, 1597, 1464, 1444, 875, 616 cm^{-1}; ^1H NMR (400 MHz, $CDCl_3$): δ_H (ppm): 7.68 (dd, J = 7.9, 1.8 Hz, 1H), 7.49 (m, 3H), 7.41 (m, 6H), 7.19 (d, J = 7.8 Hz, 2H), 7.09 (m, 3H), 6.94 (d, J = 15.6 Hz, 1H), 6.86 (dd, J = 15.5, 10.7 Hz, 1H), 5.16 (s, 2H) (Fig. S26); ^{13}C NMR (100 MHz, $CDCl_3$): δ_c (ppm): 192.73, 157.39, 142.97, 140.79, 136.35, 133.43, 132.82, 131.11, 130.55, 129.64, 129.25, 128.97, 128.80, 127.38, 127.33, 127.16, 121.08, 113.19, 70.66 (Fig. S27); LC-MS: positive ion mode: m/z = 419.0634 $[M]^+$ calculated mass (M) for $C_{24}H_{19}BrO_2$ is 419.3180 (Fig. S28).

3.3.10 2-((2-((2*E*,4*E*)-5-Phenylpenta-2,4-dienoyl)phenoxy) methyl) benzonitrile (5i). Yield: 302 mg (89%), yellow solid, m.p. 137–139 °C; IR (KBr): 3764, 3400, 3031, 3014, 2960, 2732, 2716, 2597,2513, 2303, 1482 cm^{-1}; ^1H NMR (400 MHz, $CDCl_3$): δ_H (ppm): 7.90 (dd, J = 7.7, 0.9 Hz, 1H), 7.75 (m, 2H), 7.64 (m, 5H), 7.43 (m, 4H), 7.24 (dd, J = 15.1, 10.6 Hz, 2H), 7.12 (ddd, J = 12.7, 5.6, 2.9 Hz, 2H), 6.97 (dd, J = 42.3, 12.9 Hz, 1H), 5.38 (s, 2H) (Fig. S29); ^{13}C NMR (100 MHz, $CDCl_3$): δ_c (ppm): 192.38, 156.27, 143.26, 141.11, 139.59, 135.95, 133.13, 132.76, 130.62, 130.04, 129.66, 129.04, 128.80, 128.76, 127.07, 126.81, 121.54, 116.94, 113.08, 111.03, 68.20 (Fig. S30); LC-MS: positive ion mode: m/z = 366.1500 $[M + H]^+$ calculated mass (M) for $C_{25}H_{19}NO_2$ is 365.4320 (Fig. S31).

3.3.11 (2*E*,4*E*)-1-(2-((4-Methylbenzyl)oxy)phenyl)-5-phenylpenta-2,4-dien-1-one (5j). Yield: 288 mg (85%), yellow solid, m.p. 184–186 °C; IR (KBr): 3327, 2922, 2860, 2338, 1739, 1599, 1412, 1112, 971, 711, 636 cm^{-1}; ^1H NMR (400 MHz, $CDCl_3$): δ_H (ppm): 7.58 (m, 6H), 7.43 (m, 5H), 7.31 (m, 2H), 7.11 (m, 3H), 6.95 (d, J = 15.1 Hz, 1H), 5.23 (s, 2H), 2.50 (dt, J = 3.6, 1.8 Hz, 3H) (Fig. S32); ^{13}C NMR (100 MHz, $CDCl_3$): δ_c (ppm): 192.70, 163.59, 145.50, 142.91, 136.23, 135.97, 129.50, 129.24, 128.91, 128.79, 127.44, 127.36, 127.15, 126.69, 123.49, 121.10, 120.03, 118.78, 118.60, 70.78, 21.14 (Fig. S33); LC-MS: positive ion mode: m/z = 355.1691 $[M + H]^+$ calculated mass (M) for $C_{25}H_{22}O_2$ is 354.4490 (Fig. S34).

3.3.12 (2*E*,4*E*)-1-(2-(Benzyloxy)phenyl)-5-phenylpenta-2,4-dien-1-one (5k). Yield: 324 mg (92%), yellow solid, m.p. 225–227 °C; IR (KBr): 3759, 3448, 2993, 2735, 2725, 2492, 2448, 1577, 477, 467 cm^{-1}; ^1H NMR (400 MHz, $CDCl_3$): δ_H (ppm): 7.67 (dd, J = 7.6, 1.8 Hz, 1H), 7.52 (m, 5H), 7.43 (m, 6H), 7.07 (td, J = 8.3, 2.0 Hz, 2H), 6.98 (dd, J = 25.9, 15.4 Hz, 2H), 6.87 (dd, J = 15.5, 10.7 Hz, 2H), 5.21 (s, 2H) (Fig. S35); ^{13}C NMR (100 MHz, $CDCl_3$): δ_c (ppm): 193.08, 157.21, 143.20, 140.99, 136.49, 136.29, 132.75, 130.97, 130.51, 129.73, 129.00, 128.80, 128.57, 127.96, 127.18, 121.15, 113.14, 70.65 (Fig. S36); LC-MS: positive ion mode: m/z = 341.1538 $[M + H]^+$ calculated mass (M) for $C_{24}H_{20}O_2$ is 340.4220 (Fig. S37).

3.3.13 (2*E*,4*E*)-1-(2-(Hexyloxy)phenyl)-5-phenylpenta-2,4-dien-1-one (5l). Yield: 275 mg (80%), yellow solid, m.p. 191–193 °C; IR (KBr): 3655, 3545, 3453, 3324, 3214, 3110, 2094, 1905, 1809, 543, 457 cm^{-1}; ^1H NMR (400 MHz, $CDCl_3$): δ_H (ppm): 7.63–7.54 (m, 2H), 7.51 (m, 1H), 7.46 (m, 4H), 7.27 (ddd, J = 15.1, 6.6, 3.9 Hz, 1H), 7.16 (m, 3H), 7.03 (td, J = 7.5, 0.7 Hz, 1H), 6.93 (d, J = 15.0 Hz, 1H), 4.06 (t, J = 6.1 Hz, 2H), 1.70 (dt, J = 14.5, 6.2 Hz, 2H), 1.43 (m, 2H), 1.27 (m, 4H), 0.76 (t, J = 7.1 Hz, 3H) (Fig. S38); LC-MS: positive ion mode: m/z = 335.2002 $[M + H]^+$ calculated mass (M) for $C_{23}H_{26}O_2$ is 334.4590 (Fig. S39).

3.3.14 (2*E*,4*E*)-1-(2-(Pentyloxy)phenyl)-5-phenylpenta-2,4-dien-1-one (5m). Yield: 281 mg (81%), yellow solid, m.p. 238–240 °C; IR (KBr): 3216, 3199, 3182, 2453, 1967, 1319, 804, 525, 523 cm^{-1}; ^1H NMR (400 MHz, $CDCl_3$): δ_H (ppm): 7.58 (m, 2H), 7.52 (m, 2H), 7.38 (tdd, J = 6.1, 3.9, 2.4 Hz, 1H), 7.31 (m, 3H), 7.16 (dd, J = 14.0, 9.0 Hz, 2H), 7.03 (td, J = 7.5, 0.9 Hz, 3H), 6.93 (d, J = 15.0 Hz, 1H), 4.06 (t, J = 6.2 Hz, 2H), 1.71 (dq, J = 12.6, 6.3 Hz, 2H), 1.41 (m, 4H), 0.81 (t, J = 7.2 Hz, 3H) (Fig. S40); ^{13}C NMR (100 MHz, $CDCl_3$): δ_c (ppm): 192.76, 157.45, 142.62, 140.80, 136.00, 132.70, 130.71, 130.01, 129.14, 128.88, 128.66, 126.98, 120.36, 112.32, 68.39, 28.69, 28.20, 22.20, 13.89 (Fig. S41); LC-MS: positive ion mode: m/z = 321.1863 $[M + H]^+$ calculated mass (M) for $C_{22}H_{24}O_2$ is 320.4320 (Fig. S42).

3.3.15 (2*E*,4*E*)-1-(2-(2-Bromoethoxy)phenyl)-5-phenylpenta-2,4-dien-1-one (5n). Yield: 250 mg (78%), yellow semi liquid; IR (KBr): 3450, 2923, 2853, 1714, 1600, 1453, 1366, 1224, 1166, 1123, 1081, 972, 909, 871, 754, 647 cm^{-1}; ^1H NMR (400 MHz, $CDCl_3$): δ_H (ppm): 7.64 (dd, J = 7.6, 1.8 Hz, 1H), 7.48 (m, 4H), 7.40 (m, 2H), 7.30 (ddd, J = 7.3, 3.6, 1.2 Hz, 1H), 7.11 (m, 2H), 7.00 (dd, J = 19.3, 8.9 Hz, 2H), 6.93 (d, J = 7.9 Hz, 1H), 4.38 (t, J = 5.9 Hz, 2H), 3.67 (t, J = 5.9 Hz, 2H) (Fig. S43); ^{13}C NMR (100 MHz, $CDCl_3$): δ_c (ppm): 192.57, 156.49, 143.44, 141.22, 136.29, 132.83, 130.79, 130.72, 129.76, 129.07, 128.84, 127.31, 127.25, 121.63, 112.65, 68.59, 29.14 (Fig. S44); LC-MS: positive ion mode: m/z = 357.0502 $[M]^+$ calculated mass (M) for $C_{19}H_{17}BrO_2$ is 357.2470 (Fig. S45).

3.4. *In vitro* cytotoxicity studies on normal and cancer cell lines

The cytotoxic activity of the synthesized cinnamaldehyde–chalcone derivatives was assessed using the MTT assay, as described in our previously published work.[45] The evaluation was conducted on four cell lines: three cancer cell lines (DU145, SKBR-3, and HepG2) and one normal cell line (HEK-293). All cell lines were obtained from the American Type Culture Collection (ATCC, Bethesda, MD, USA). Cells were cultured in Dulbecco's Modified Eagle Medium (DMEM) supplemented with 10% fetal bovine serum (FBS), 2 mM l-glutamine, and 100 μg per mL penicillin–streptomycin. Cultures were maintained in a humidified incubator at 37 °C with 5% CO_2. Initially Cells were seeded in 96-well microtiter plates at a density of 10 000 cells per well and allowed to adhere overnight. The following day, varying concentrations of the test compounds were added, and the cells were incubated for 48 hours. After the treatment period, the medium was replaced with fresh culture medium, followed by the addition of 10 μL of 12 mM MTT reagent to each well. Plates were incubated in the dark at 37 °C for 4 hours. Subsequently, 100 μL of dimethyl sulfoxide (DMSO) was added to each well to solubilize the formazan crystals formed. Absorbance was measured at 570 nm using a Multimode Varioskan Flash microplate reader (Tecan), with wells containing only media serving as blanks. Data were collected from three independent experiments, and IC_{50} values for each cell line were calculated using linear regression analysis.

3.5. Antimicrobial studies

In this study, antimicrobial activity was evaluated against six microbial strains: two Gram-negative bacteria (*Escherichia coli* MTCC 730 and *Klebsiella pneumoniae* MTCC 109), two Gram-positive bacteria (*Staphylococcus aureus* MTCC 96 and *Bacillus subtilis* MTCC 121), and two fungal strains (*Candida albicans* MTCC 227 and *Candida tropicalis* MTCC 230). All strains were obtained from the Microbial Type Culture Collection and Gene Bank (MTCC), Chandigarh. Bacterial strains were cultured on Mueller–Hinton Agar (MHA) and maintained in Mueller–Hinton Broth (MHB) at 37 °C for 24 hours, while fungal strains were maintained under similar conditions at 30 °C. The antimicrobial efficacy of the test compounds was assessed using the agar well diffusion method, in accordance with Clinical and Laboratory Standards Institute (CLSI) guidelines (2012).[46] Briefly, the inoculum was uniformly spread over the agar surface, and wells of 6–8 mm diameter were aseptically punched into the agar. Each well was loaded with 20–100 μL of the test compound. The plates were then incubated at the respective optimal temperatures for 24 hours, after which the zones of inhibition were measured to evaluate antimicrobial activity.

3.4. *In vivo* acute oral toxicity of compound 5n

The experiment was carried out following IAEC-approved protocol no. CIMAP/IAEC/2024–25/19 and methodologies recently published from the lab[47,48] for the acute oral toxicity of the most potent molecule in mouse model. The Institutional Animal Ethics Committee of CSIR- Central Institute of Medicinal & Aromatic Plants, Lucknow, UP, India is a constituent body operates under CCSEA, Government of India and regulates compliances of guidelines related to ethical use animals in experimental studies. For the acute oral toxicity study, 30 mice (15 male and 15 female) were taken and divided into five groups comprising 3 male and 3 female mice in each group weighing between 22–25 g. The animals were maintained at 22 ± 5 °C with humidity control and also on an automatic dark and light cycle of 12 hours. The animals were fed with the standard mice feed and provided *ad libitum* drinking water. Mice of group 1 (Group I) were kept as control and animals of groups 2, 3, 4 and 5 (Groups II, III & IV) were kept as experimental. The animals were acclimatized for 7 days in the experimental environment before the actual experimentation. The test compound was suspended in gum acacia and 0.7% CMC and was given at 5, 50, 300 and 1000 mg kg^{-1} body weight as a single acute oral dose to animals of groups 2, 3, 4 and 5 respectively. Control animals received only vehicle.

3.5. Erythrocyte osmotic fragility

Erythrocyte fragility was assessed using heparinized human blood [all experiments were performed in accordance with the approved procedure of the Institutional Human Ethics Committee (CIMAP/IHEC/2022/01) and Informed consents were obtained from human volunteers in this study] subjected to hypotonic phosphate-buffered saline (PBS, 10% stock) solutions with progressively decreasing concentrations, ranging from 0.85% to 0.10%.[47,48] Test compounds (1 μL) were added to the blood samples from the stock of 10 mg mL^{-1}, with quercetin as a positive control and DMSO as a negative control. The samples were incubated at 37 °C for 30 min to allow interaction with the test compounds. Following incubation, the treated cells were exposed to a series of hypotonic PBS solutions (0.85%, 0.65%, 0.4%, 0.2%, and 0.1%) and further incubated under the same conditions for 30 min with gentle agitation. Afterwards, the cell suspensions were centrifuged at 3000 rpm for 5 min at 4 °C to separate the supernatant. The degree of hemolysis was then quantified spectrophotometrically by measuring absorbance at 540 nm. The percentage of hemolysis was determined by calculating the ratio of the optical density (OD) of the supernatant obtained from each PBS concentration to the OD of a standard representing 100% hemolysis. Osmotic fragility curves were generated by plotting the hemolysis percentage against PBS concentration, and the mean erythrocyte fragility (MEF_{50}) was computed using Table Curve 2D Windows v4.07 (AISN Software Inc., USA).

3.6. *In silico* docking of compound 5n

3.6.1 Preparation of receptor. The 3D crystal structures of receptor protein succinate dehydrogenase (6VAX), have been acquired from the RCSB Protein Data Bank. The PDB files obtained were processed using the BIOVIA Discovery Studio 3.5 software to eliminate ligands, water molecules, and unwanted heteroatoms that could potentially hinder the docking study. The missing residues of protein molecules were repaired using Autodock tools.[49] Further polar hydrogen atoms were included to enhance the stability of the binding complexes.

3.6.2 Preparation of Ligand. The chemical structure of the synthesized compound was depicted using ChemDraw Ultra 7.0 software. The designed structure was saved in the MDL Molfile format. The inhibitor's 3D structures have been retrieved from the PubChem database in SDF file format.[50] The compounds and inhibitors MDL Molfile and SDF file were converted into the PDB file using the OpenBabel-3.1.1 software to facilitate further studies.

3.6.3 Molecular docking. Receptor-ligand interactions were studied using PyRx's AutoDock (V. 4.0). The process began with preparing a receptor protein by removing water and adding polar hydrogen and Kollman charges. Ligands rotatable bonds were set to rotate, and Gasteiger charges were calculated. Each ligand was uploaded, energy minimized, and converted to PDBQT format. A grid box was established for docking, using AutoGrid to create a grid map.[50] Rigid-flexible docking produced ten conformations, selecting the one with the most negative binding energy and RMSD values below 1.0 Å. The inhibition constant (K_i) was then calculated. BIOVIA Discovery Studio 3.5 analysed the binding pocket and ligand poses, revealing specific binding sites and interaction types.

4. Conclusion

This study successfully synthesized novel cinnamaldehyde–chalcone analogues (**5a–5n**) and evaluated their anticancer, antibacterial, and antifungal activities. Bromoethane chalcone (**5n**) showed the strongest cytotoxicity against DU145, SKBR-3, and HEPG2 cancer cell lines. Molecular docking studies revealed that compound **5n** binds strongly to succinate dehydrogenase (SDH), suggesting anticancer potential. Despite not showing good antimicrobial properties, acute oral toxicity studies in Swiss albino mice confirmed the safety of **5n** up to 1000 mg kg^{-1}. These findings highlight compound **5n** as a promising candidate for further preclinical anticancer research due to its strong cytotoxicity, favourable docking interactions, and excellent safety profile.

Author contributions

ANK performed the synthetic protocol and wrote the first draft of the manuscript; GS performed the synthetic experiments; VK and SM performed the anti-cancer activity; KS, SK and DC performed the acute oral toxicity profile; JKK and KVNSS edited the manuscript and formatted the last version; AS and AM performed molecular docking studies; NM and SL performed erythrocyte osmotic fragility analysis; BB performed the spectral analysis.

Conflicts of interest

Authors declare no conflict of interest.

Data availability

The data supporting this article have been included as part of the SI.

The supplementary material includes experimental data and spectroscopy data of all the synthesized compounds such as IR, NMR and mass. See DOI: **https://doi.org/10.1039/d5ra03706a**.

Acknowledgements

The authors thank CSIR for the grant of the Aroma Mission Phase III (HCP-0007) Project and the Director, CSIR-CIMAP, Lucknow, India, for his constant encouragement and support. CIMAP Publication Communication Number: CIMAP/PUB/2025/26.

References

1 F. Usai, A. Di Sotto and A. trans, Cinnamaldehyde as a Novel Candidate to Overcome Bacterial Resistance: An Overview of In Vitro Studies, *Antibiotics*, 2023, **12**, 254, DOI: **10.3390/antibiotics12020254**.

2 N. G. Vasconcelos, J. Croda and S. Simionatto, Antibacterial mechanisms of cinnamon and its constituents: A review, *Microb. Pathog.*, 2018, **120**, 198–203, DOI: 10.1016/j.micpath.2018.04.036.

3 N. Yossa, J. Patel, P. Millner and Y. M. Lo, Essential oils reduce *Escherichia coli* O157:H7 and *Salmonella* on spinach leaves, *J. Food Prot.*, 2012, **75**, 488–496, DOI: 10.4315/0362-028X.JFP-11-344.

4 J. Visvalingam, J. D. Hernandez -Doria and R. A. Holley, Examination of the Genome -Wide Transcriptional Response of Escherichia coli O157:H7 to Cinnamaldehyde Exposure, *Appl. Environ. Microbiol.*, 2013, **79**, 942–950, DOI: 10.1128/AEM.02767-12.

5 M. Friedman, Chemistry, Antimicrobial Mechanisms, and Antibiotic Activities of Cinnamaldehyde against Pathogenic Bacteria in Animal Feeds and Human Foods, *J. Agric. Food Chem.*, 2017, **65**, 10406–10423, DOI: 10.1021/acs.jafc.7b04344.

6 S. Qu, K. Yang, L. Chen, M. Liu, Q. Geng, X. He, Y. Li, Y. Liu and J. Tian Cinnamaldehyde, a promising natural preservative against Aspergillus flavus, *Front. Microbiol.*, 2019, **10**, 2895, DOI: 10.3389/fmicb.2019.02895.

7 Z. Hong, K. M. Talib, K. G. Mujtaba, H. Dabin, F. Yahya, Z. Congying and W. Fukaiet al, Antifungal potential of cinnamon essential oils against *Phytophthora colocasiae* causing taro leaf blight, *Chem. Biol. Technol. Agric.*, 2021, **8**, 39, DOI: 10.1186/s40538-021-00238-3.

8 L. Zhu, C. Olsen, T. McHugh, M. Friedman, D. Jaroni and S. Ravishankar, Apple, Carrot, and Hibiscus Edible Films Containing the Plant Antimicrobials Carvacrol and Cinnamaldehyde Inactivate Salmonella Newport on Organic Leafy Greens in Sealed Plastic Bags, *J. Food Sci.*, 2014, **79**, M61–M66, DOI: 10.1111/1750-3841.12318.

9 T. F. He, Z. H. Zhang, X. A. Zeng, L. H. Wang and C. S. Brennan, Determination of membrane disruption and genomic DNA binding of cinnamaldehyde to *Escherichia coli* by use of microbiological and spectroscopic techniques, *J. Photochem. Photobiol., B*, 2018, **178**, 623–630, DOI: 10.1016/j.jphotobiol.2017.11.015.

10 B. J. Chen, C. S. Fu, G. H. Li, X. N. Wang, H. X. Lou, D. M. Ren and T. Shen, Cinnamaldehyde Analogues as Potential Therapeutic Agents, *Mini Rev. Med. Chem.*, 2017, **17**, 33–43, DOI: 10.2174/1389557516666160121120744.

11 H.-S. Lee, S.-Y. Kim, C.-H. Lee and Y.-J. Ahn, Cytotoxic and mutagenic effects of Cinnamomum cassia bark -derived materials, *J. Microbiol. Biotechnol.*, 2004, **14**, 1176–1181.

12 M. A. Lee, H. J. Park, H.-J. Chung, W. K. Kim and S. K. Lee, Antitumor Activity of 2 - Hydroxycinnamaldehyde for Human Colon Cancer Cells through Suppression of β - Catenin Signaling, *J. Nat. Prod.*, 2013, **76**, 1278–1284, DOI: 10.1021/np400216m.

13 W. Xue, J. Liu, X. Xu, C. Chen, B. Wei and Y. Zhao, Cardioprotective effect of Cinnamamide derivative compound 10 against myocardial ischemia-reperfusion through regulating cardiac autophagy via Sirt1, *Biomed. Pharmacother.*, 2024, **176**, 116819, DOI: 10.1016/j.biopha.2024.116819.

14 W. X. Cheng, S. Zhong, X. B. Meng, N. Y. Zheng, P. Zhang, Y. Wang, L. Qin and X. L. Wang, Cinnamaldehyde Inhibits Inflammation of Human Synoviocyte Cells Through Regulation of Jak/Stat Pathway and Ameliorates Collagen-Induced Arthritis in Rats, *J. Pharmacol. Exp. Therapeut.*, 2020, **373**(2), 302–310, DOI: 10.1124/jpet.119.262907.

15 Y. Long, J. Xu, Z. Hu, X. Y. Fan and H. Wang, Antifungal activity of Cinnamaldehyde derivatives against fluconazole-resistant Candida albicans, *Microb Pathog.*, 2024, **195**, 106877, DOI: 10.1016/j.micpath.2024.106877.

16 C. Pandit and K. R. Anilakumar, Cold adaptive thermogenesis following consumption of certain pungent spice principles: A validation study, *J. Therm. Biol.*, 2017, **64**, 35–40, DOI: 10.1016/j.jtherbio.2016.12.008.

17 W. C. Chai, J. J. Whittall, S. W. Polyak, K. Foo, X. Li, C. J. Dutschke, A. D. Ogunniyi, S. Ma, M. J. Sykes, S. J. Semple and H. Venter, Cinnamaldehyde derivatives act as antimicrobial agents against *Acinetobacter baumannii* through the inhibition of cell division, *Front. Microbiol.*, 2022, **29**(13), 967949, DOI: 10.3389/fmicb.2022.

18 X. H. Gao, J. J. Tang, H. R. Liu, L. B. Liu and Y. Z. Liu, Structure–activity study of fluorine or chlorine-substituted cinnamic acid derivatives with tertiary amine side chain in acetylcholinesterase and butyrylcholinesterase inhibition, *Drug Dev. Res.*, 2019, **80**, 438–445, DOI: 10.1002/ddr.21515.

19 M. S. Alam, S. M. Rahman and D.-U. Lee, Synthesis, biological evaluation, quantitative-SAR and docking studies of novel chalcone derivatives as antibacterial and antioxidant agents, *Chem. Pap.*, 2015, **69**(8), 1118–1129, DOI: 10.1515/chempap-2015-0113.

20 R. W. Wadleigh and S. J. Yu, Glutathione transferase activity of fall armyworm larvae toward α, β-unsaturated carbonyl allelochemicals and its induction by allelochemicals, *Insect Biochem.*, 1987, **17**(5), 759–764, DOI: 10.1016/0020-1790(87)90046-1.

21 C. Karthikeyan, N. S. H. Narayana Moorthy, S. Ramasamy, U. Vanam, E. Manivannan, D. Karunagaran and P. Trivedi, Advances in chalcones with anticancer activities, *Recent Pat. Anticancer Drug Discov.*, 2014, **10**(1), 97–115, DOI: 10.2174/1574892809666140819153902.

22 M. Ninomiya and M. Koketsu, in*Natural Products Ramawat*, Springer Verlag, Berlin, 2013.

23 Y. Ouyang, J. Li, X. Chen, X. Fu, S. Sun and Q. Wu, Chalcone derivatives: role in anticancer therapy, *Biomolecules*, 2021, **11**(6), 894–1020, DOI: 10.3390/biom11060894.

24 H.-L. Qin, Z.-W. Zhang, R. Lekkala, H. Alsulami and K. Rakesh, Chalcone hybrids as privileged scaffolds in antimalarial drug discovery: a key review, *Eur. J. Med. Chem.*, 2020, **193**, 112215, DOI: 10.1016/j.ejmech.2020.112215.

25 S. Welday Kahssay, G. S. Hailu and K. Taye Desta, Design, Synthesis, Characterization and in vivo Antidiabetic Activity Evaluation of Some Chalcone Derivatives, *Drug Des. Dev. Ther.*, 2021, **15**, 3119–3129, DOI: 10.2147/DDDT.S316185.

26 N. Fakhrudin, K. K. Pertiwi, M. I. Takubessi, E. F. Susiani, A. Nurrochmad, S. Widyarini, A. Sudarmanto,

A. A. Nugroho and S. Wahyuono, A geranylated chalcone with antiplatelet activity from the leaves of breadfruit (*Artocarpus altilis*), *Pharmacia*, 2020, **67**, 173–180, DOI: 10.3897/pharmacia.67.e56788.

27 T. S. Ibrahim, A. H. Moustafa, A. J. Almalki, R. M. Allam, A. Althagafi, S. Md and M. F. Mohamed, Novel chalcone/aryl carboximidamide hybrids as potent anti-inflammatory via inhibition of prostaglandin E2 and inducible NO synthase activities: design, synthesis, molecular docking studies and ADMET prediction, *J. Enzym. Inhib. Med. Chem.*, 2021, **36**(1), 1067–1078, DOI: 10.1080/14756366.2021.1929201.

28 S. Murtaza, K. Z. Mir, A. Tatheerb and R. S. Ullah, Synthesis and evaluation of chalcone and its derivatives as potential anticholinergic agents, *Lett. Drug Des. Discovery*, 2019, **16**(3), 322–332, DOI: 10.2174/1570180815666180523085436.

29 P. Bhoj, N. Togre, S. Bahekar, K. Goswami, H. Chandak and M. Patil, Immunomodulatory Activity of Sulfonamide Chalcone Compounds in Mice Infected with Filarial Parasite, Brugia malayi, *Indian J. Clin. Biochem.*, 2019, **34**(2), 225–229, DOI: 10.1007/s12291-017-0727-5.

30 B. Lakshminarayanan, N. Kannappan and T. Subburaju, Synthesis and biological evaluation of novel chalcones with methanesulfonyl end as potent analgesic and anti-inflammatory agents, *Int. J. Pharmaceutical Res. Biosci.*, 2020, **11**(10), 4974–4981, DOI: 10.13040/IJPSR.0975-8232.11(10).4974-81.

31 E. N. Okolo, D. I. Ugwu, B. E. Ezema, J. C. Ndefo, F. U. Eze, C. G. Ezema, J. A. Ezugwu and O. T. Ujam, New chalcone derivatives as potential antimicrobial and antioxidant agent, *Sci. Rep.*, 2021, **11**, 21871, DOI: 10.1038/s41598-021-01292-5.

32 M. R. Reddy, I. S. Aidhen, U. A. Reddy, G. B. Reddy, K. Ingle and S. Mukhopadhyay, Synthesis of 4-C-β-D-Glucosylated Isoliquiritigenin and Analogues for Aldose Reductase Inhibition Studies, *Eur. J. Org Chem.*, 2019, **24**, 3937–3948, DOI: 10.1002/ejoc.201900413.

33 G. Aljohani, A. Al-Sheikh Ali, S. Y. Alraqa, S. Itri Amran and N. Basar, Synthesis, molecular docking and biochemical analysis of aminoalkylated naphthalene-based chalcones as acetylcholinesterase inhibitors, *J. Taibah Univ. Sci.*, 2021, **15**(1), 781–797, DOI: 10.1080/16583655.2021.2005921.

34 N. Duran, M. F. Polat, D. A. Aktas, M. A. Alagoz, E. Ay, F. Cimen, E. Tek, B. Anil and S. Algul, New chalcone derivatives as effective against SARS-CoV-2 agent, O, *Int. J. Clin. Pract.*, 2021, 14846, DOI: 10.1111/ijcp.14846.

35 T. H. Bui, N. T. Nguyen, P. H. Dang, H. X. Nguyen and M. T. T. Nguyen, Design and synthesis of chalcone derivatives as potential non-purine xanthine oxidase inhibitors, *SpringerPlus*, 2016, **5**(1), 1789, DOI: 10.1186/s40064-016-3485-6.

36 L. Kang, X. H. Gao, H. R. Liu, X. Men, H. N. Wu, P. W. Cui, E. Oldfield and J. Y. Yan, Structure–activity relationship investigation of coumarin–chalcone hybrids with diverse side-chains as acetylcholinesterase and butyrylcholinesterase inhibitors, *Mol. Divers.*, 2018, **22**, 893–906, DOI: 10.1007/s11030-018-9839-y.

37 Ch. Yakaiah, T. Sneha, T. Shalini, S. Chinde, D. A. Kumar, A. N. Kumar, K. V. N. S. Srinivas, S. Alam, J. K. Kumar, F. Khan, A. Tiwari and P. Grover, Synthesis, docking and ADMET studies of novel chalcone triazoles for anticancer and anti-diabetic activity, *Eur. J. Med. Chem.*, 2015, **93**, 564–573, DOI: 10.1016/j.ejmech.2015.02.027.

38 B. Komuraiah, A. Niranjana Kumar, K. V. N. S. Srinivas, J. Kotesh Kumar, C. Srinivas, K. D. Anand, K. Yogesh, G. Paramjit, T. Ashok and K. Feroz, Synthesis and bioactivity evaluation of eugenol hybrids obtained by Mannich and 1,3 dipolar cycloaddition reactions, *J. Heterocycl. Chem.*, 2021, **58**(11), 2078–2089, DOI: 10.1002/jhet.4331.

39 E. Mallikarjun, D. Suneesha, A. Niranjana Kumar, S. Akanksha, D. Hashnu, J. Kotesh Kumar, K. V. N. S. Srinivas, M. Abha, B. Venkatesh, J. Nishant, S. Sravanthi and T. Radhika, Synthesis of novel anticancer coumarin-triazole-chalcone hybrids as potential AKT inhibitors, *Indian J. Chem.*, 2023, **62**, 1162, DOI: 10.56042/ijc.v62i11.2610.

40 H. Iqbal, A. K. Verma, P. Yadav, A. Sarfaraz, M. Shafiq, M. Divya, F. Khan, K. Hanif, A. S. Negi and D. Chanda, Antihypertensive Effect of a Novel Angiotensin II Receptor Blocker Fluorophenyl Benzimidazole: Contribution of cGMP, Voltage-dependent Calcium Channels, and BK_{Ca} Channels to Vasorelaxant Mechanisms, *Front. Pharmacol*, 2021, **12**, 611109, DOI: 10.3389/fphar.2021.611109.

41 T. Huang, Y. Chen, Q. Zhao, X. Wu, H. Li, X. Luo, Y. Su, S. Zhang, P. Liu and N. Tang, Dual Regulation of Sprouty 4 Palmitoylation by ZDHHC7 and Palmitoyl-Protein Thioesterase 1: A Potential Therapeutic Strategy for Cisplatin-Resistant Osteosarcoma, *Research*, 2025, 0708, DOI: 10.34133/research.0708.

42 J. Singh and A. Meena, Exploration of Chemopreventive Potential of Linalool in Targeting Lung Cancer Biomarkers, *Endocr. Metab. Immune Disord. - Drug Targets*, 2022, **22**(14), 1416–1424, DOI: 10.2174/1871530321666210909165426.

43 T. Zhao, X. Mu and Q. You, Succinate: An initiator in tumorigenesis and progression, *Oncotarget*, 2017, **8**, 53819–53828, DOI: 10.18632/oncotarget.17734.

44 L. Valls-Lacalle, I. Barba, E. Miró-Casas, J. Alburquerque-Béjar, M. Ruiz-Meana, M. Fuertes-Agudo, A. Rodríguez-Sinovas and D. García-Dorado, Succinate dehydrogenase inhibition with malonate during reperfusion reduces infarct size by preventing mitochondrial permeability transition, *Cardiovasc. Res.*, 2016, **109**(3), 374–384, DOI: 10.1093/cvr/cvv279.

45 S. S. Deshpande, D. Veeragoni, L. Kongari, J. Mamilla and S. Misra, Synthesis of biocompatible chitosan coated TiO2-curcumin nanocomposites shows potent anticancer activity towards melanoma cancer cells, *J. Drug Delivery Sci. Technol.*, 2023, **1**(85), 104592, DOI: 10.1016/j.jddst.2023.104592.

46 CLSI, *Performance Standards for Antimicrobial Disk Susceptibility Tests, Approved Standard*, Clinical and Laboratory Standards Institute, 950 West Valley Road, Suite 2500, Wayne, Pennsylvania 19087, USA, 7th edn, 2012.

47 K. Fatima, Z. A. Wani, A. Meena and S. Luqman, Geraniol exerts its antiproliferative action by modulating molecular targets in lung and skin carcinoma cells, *Phytother Res.*, 2021, **35**(7), 3861–3874, DOI: **10.1002/ptr.7094**.

48 S. Luqman, K. O. Prabu, A. Pal, D. Saikia, M. P. Darokar and S. P. Khanuja, Antibiotic-Induced Alterations in the Osmotic Resistance of Erythrocytes is Modulated by β-Carotene and L –Ascorbic Acid, *Nat. Prod. Commun.*, 2006, **1**(6), 1934578X0600100610.

49 A. Singh, A. Mishra, A. Meena, N. Mishra and S. Luqman, Exploration of selected monoterpenes as potential TRPC channel family modulator in lung cancer, an *in-silico* upshot, *J. Biomol. Struct. Dyn.s*, 2023, **42**(15), 7917–7933, DOI: **10.1080/07391102.2023.2241900**.

50 A. Mathur, A. Singh, Y. Hussain, A. Mishra, A. Meena, N. Mishra and S. Luqman, Regulating pri/pre-microRNA up/down expressed in cancer proliferation, angiogenesis and metastasis using selected potent triterpenoids, *Int. J. Biol. Macromol.*, 2024, **257**, 127945, DOI: **10.1016/j.ijbiomac.2023.127945**.